

Non-iterative phase hologram computation for low speckle holographic image projection

Deniz Mengü, Erdem Ulusoy, and Hakan Urey*

*Optical Microsystems Laboratory, Department of Electrical Engineering, Koç University,
TR-34450, Istanbul, Turkey*

[*hurey@ku.edu.tr](mailto:hurey@ku.edu.tr)

Abstract: Phase-only spatial light modulators (SLMs) are widely used in holographic display applications, including holographic image projection (HIP). Most phase computer generated hologram (CGH) calculation algorithms have an iterative structure with a high computational load, and also are prone to speckle noise, as a result of the random phase terms applied on the desired images to mitigate the encoding noise. In this paper, we present a non-iterative algorithm, where simple Discrete Fourier Transform (DFT) relations are exploited to compute phase CGHs that exactly control half of the desired image samples (those on even - or odd - indexed rows - or columns) via a single Fast Fourier Transform (FFT) and trivial arithmetic operations. The encoding noise appearing on the uncontrolled half of the image samples is reduced by the application of structured, non-random initial phase terms so that speckle noise is also kept low. High quality reconstructions are obtained under temporal averaging of several SLM frames. Interlaced video within half of the addressable image area is readily deliverable without frame rate division. Our algorithm provides about 6X and 20X reduction in computational cost compared to IFTA and FIDOC algorithms, respectively. Simulations and experiments verify that the algorithm constitutes a promising option for real-time computation of phase CGHs.

© 2016 Optical Society of America

OCIS codes: (090.1760) Computer holography; (070.6120) Spatial light modulators; (090.2870) Holographic display.

References and links

1. A. W. Lohmann, and D. P. Paris, "Binary Fraunhofer holograms, generated by computer," *Appl. Opt.* **6**(10), 1739–1748 (1967).
2. L. B. Lesem, P. M. Hirsch, and J. A. Jordan, "The kinoform: a new wavefront reconstruction device," *IBM J. Res. Dev.* **13**(2), 150–155 (1969).
3. B. R. Brown, and A. W. Lohmann, "Computer-generated binary holograms," *IBM J. Res. Dev.* **13**(2), 160–168 (1969).
4. M. Reicherter, T. Haist, E. U. Wagemann, and H. J. Tiziani, "Optical particle trapping with computer-generated holograms written on a liquid-crystal display," *Opt. Lett.* **24**(9), 608–610 (1999).
5. T. Nobukawa, Y. Wani, and T. Nomura, "Multiplexed recording with uncorrelated computer-generated reference patterns in coaxial holographic data storage," *Opt. Lett.* **40**(10), 2161–2164 (2015).
6. I. Dolev, I. Epstein, and A. Arie, "Surface-plasmon holographic beam shaping," *Phys. Rev. Lett.* **109**(20), 203903 (2012).

7. K. Y. Hsu, H. Y. Li, and D. Psaltis, "Holographic implementation of a fully connected neural network," in *Proceedings of the IEEE* (IEEE, 1990) **78**(10), pp. 1637–1645.
8. M. A. A. Neil, M. J. Booth, and T. Wilson, "Dynamic wave-front generation for the characterization and testing of optical systems," *Opt. Lett.* **23**(23), 1849–1851 (1998).
9. M. Makowski, M. Sypek, I. Ducin, A. Fajst, A. Siemion, J. Suszek, and A. Kolodziejczyk, "Experimental evaluation of a full-color compact lensless holographic display," *Opt. Express* **17**(23), 20840–20846 (2009).
10. A. Georgiou, J. Christmas, N. Collings, J. Moore, and W. A. Crossland, "Aspects of hologram calculation for video frames," *J. Opt. A Pure Appl. Opt.* **10**, 035302 (2008).
11. E. Buckley, "Holographic laser projection," *J. Disp. Technol.* **7**(3), 135–140 (2011).
12. E. Buckley, "Holographic projector using one lens," *Opt. Lett.* **35**(20), 3399–3401 (2010).
13. A. Georgiou, J. Christmas, J. Moore, A. Jeziorska-Chapman, A. Davey, N. Collings, and W. A. Crossland, "Liquid crystal over silicon device characteristics for holographic projection of high-definition television images," *Appl. Opt.* **47**(26), 4793–4803 (2008).
14. U. Efron, *Spatial Light Modulator Technology: Materials, Devices, and Applications* (Marcel Dekker, 1994).
15. G. Lazarev, A. Hermerschmidt, S. Krüger, and S. Osten, "LCOS spatial light modulators: Trends and applications," in *Optical Imaging and Metrology: Advanced Technologies*, W. Osten, and N. Reingand, eds. (Wiley-VCH, 2012), chap. 1, pp. 130.
16. R. Tudela, E. Martin-Badosa, I. Labastida, S. Vallmitjana, I. Juvells, and A. Carnicer, "Full complex Fresnel holograms displayed on liquid crystal devices," *J. Opt. A Pure Appl. Opt.* **5**(5), s189 (2003).
17. A. Shibukawa, A. Okamoto, Y. Goto, S. Honma, and A. Tomita, "Digital phase conjugate mirror by parallel arrangement of two phase-only spatial light modulators," *Opt. Express* **22**(10), 11918–11929 (2014).
18. V. Arrizón, G. Méndez, and D. Sánchez-de-La-Llave, "Accurate encoding of arbitrary complex fields with amplitude-only liquid crystal spatial light modulators," *Opt. Express* **13**(20), 7913–7927 (2005).
19. F. Mok, J. Diep, H. K. Liu, and D. Psaltis, "Real-time computer-generated hologram by means of liquid-crystal television spatial light modulator," *Opt. Lett.* **11**(11), 748–750 (1986).
20. M. A. Seldowitz, J. P. Allebach, and D. W. Sweeney, "Synthesis of digital holograms by direct binary search," *Appl. Opt.* **26**(14), 2788–2798 (1987).
21. E. Ulusoy, L. Onural, and H. M. Ozaktas, "Synthesis of three-dimensional light fields with binary spatial light modulators," *J. Opt. Soc. Am. A* **28**(6), 1211–1223 (2011).
22. S. Weissbach, and F. Wyrowski, "Error diffusion procedure: theory and applications in optical signal processing," *Appl. Opt.* **31**(14), 2518–2534 (1992).
23. F. Wyrowski, "Diffractive optical elements: iterative calculation of quantized, blazed phase structures," *J. Opt. Soc. Am. A* **7**(6), 961–969 (1990).
24. J. R. Fienup, "Phase retrieval algorithms: a comparison," *Appl. Opt.* **21**(15), 2758–2769 (1982).
25. J. R. Fienup, "Reconstruction of an object from the modulus of its Fourier transform," *Opt. Lett.* **3**(1), 27–29 (1978).
26. J. R. Fienup, "Iterative method applied to image reconstruction and to computer-generated holograms," *Opt. Eng.* **19**(3), 193297 (1980).
27. R. Liu, B. Y. Gu, B. Z. Dong, and G. Z. Yang, "Design of diffractive phase elements that realize axial-intensity modulation based on the conjugate-gradient method," *J. Opt. Soc. Am. A* **15**(3), 689–694 (1998).
28. K. V. Chellappan, E. Erden, and H. Urey, "Laser-based displays: a review," *Appl. Opt.* **49**(25), F79–F98 (2010).
29. F. Wyrowski, and O. Bryngdahl, "Speckle-free reconstruction in digital holography," *J. Opt. Soc. Am. A* **6**(8), 1171–1174 (1989).
30. D. Mengu, E. Ulusoy, and H. Urey, "Holographic Image Projection with Phase Only Spatial Light Modulators via Non-Iterative CGH Computation Method," In *Digital Holography and Three-Dimensional Imaging Conference*, (Optical Society of America, 2015), pp. DT2A-5.
31. C. K. Hsueh, and A. A. Sawchuk, "Computer-generated double-phase holograms," *Appl. Opt.* **17**(24), 3874–3883 (1978).
32. D. Abookasis, and J. Rosen, "Three types of computer-generated hologram synthesized from multiple angular viewpoints of a three-dimensional scene," *Appl. Opt.* **45**(25), 6533–6538 (2006).
33. F. Wyrowski, and O. Bryngdahl, "Iterative Fourier-transform algorithm applied to computer holography," *J. Opt. Soc. Am. A* **5**(7), 1058–1065 (1988).
34. T. Shimobaba, and T. Ito, "Random phase-free computer-generated hologram," *Opt. Express* **23**(7), 9549–9554 (2015).
35. T. Shimobaba, T. Kakue, Y. Endo, R. Hirayama, D. Hiyama, S. Hasegawa, Y. Nagahama, M. Sano, T. Sugie, and T. Ito, "Random phase-free kinoform for large objects," *Opt. Express* **23**(13), 17269–17274 (2015).
36. Z. Wang, A. C. Bovik, H. R. Sheikh, and E. P. Simoncelli, "Image quality assessment: from error visibility to structural similarity," *IEEE T. Image Process.* **13**(4), 600–612 (2004).
37. J. Yan, Y. Xing, Z. Guo, and Q. Li, "Low voltage and high resolution phase modulator based on blue phase liquid crystals with external compact optical system," *Opt. Express* **23**(12), 15256–15264 (2015).

1. Introduction

Computer-generated holograms (CGHs) have been researched for almost 50 years [1]. In the early times, CGHs were implemented by printed binary masks or kinoforms [2, 3]. With the advances in the spatial light modulator (SLM) technology, CGHs are now widely used in dynamic applications such as optical tweezers, beam shaping, optical information processing, optical data storage, optical communications, adaptive optics, wave-front correction and holographic displays [4–8]. CGHs are also used in holographic image projection (HIP), which has been receiving increasing interest over conventional image projection due to superior light efficiency, lensless projection ability, and easier aberration compensation capability [9–13].

CGHs are ideally complex valued functions that modulate both the amplitude and phase of the incident light. Yet, available SLMs can provide only some restricted type of modulation, such as phase-only, amplitude-only or binary [14, 15]. One option is to perform direct quantization on the ideal full complex CGH. This easiest option results in high levels of noise, and in general is quite sub-optimal. Hence, SLM restrictions are handled via more sophisticated approaches, which can be categorized into two. In the first approach, several restricted-type SLMs are used in combination to achieve a system that provides full-complex modulation. An example is to image an amplitude-only SLM on a phase-only SLM [16]. Another is to superpose coherent beams from two phase-only SLMs [17]. Such schemes, however, have complicated optical setups and require high precision alignment. They thus have limited utility.

The second approach encodes the ideal full-complex CGH into a restricted type CGH that can be displayed on the SLM. As a result of the encoding process, the SLM output consists of a noise beam along with the desired beam. The encoding procedures are usually tuned so that the noise beam has reduced energy, or gets spatially separated from the desired beam in the course of propagation. Many algorithms are proposed for various SLM types. [18, 19] investigate the CGH computation for amplitude-only and amplitude mostly SLMs, while [20, 21] explore the binary SLM case. Most algorithms, however, are proposed for phase-only SLMs, due to their superior light efficiency and multilevel modulation capability [22–27]. These algorithms perform successful encodings. Yet, almost all of them have an iterative structure and involve repetitive Fast Fourier Transform (FFT) or pixel-by-pixel processing operations that pose significant computational complexity. In spite of the improvements in the computational power and parallel processing hardware such as FPGAs and GPUs, real-time operations still remain as a challenge due to lack of non-iterative direct solutions.

Another disadvantage of most established phase CGH computation algorithms, especially in the HIP context, is related to speckle noise. As well known, all laser based display systems are prone to speckle noise to some degree [28]. In HIP, speckle partly results due to physical factors such as the surface roughness of optical components or projection screens, and partly due to the CGH computation procedure. In particular, most algorithms converge to a solution by assigning random phase values to the desired image samples, leading to speckled reconstructions even if physical factors of speckle are removed. Some algorithms limit the phase variation during iterations to achieve speckle reduction, but at the cost of slower convergence and increased computational cost [29].

In this paper, we present a non-iterative phase CGH computation algorithm which is particularly suitable for real-time HIP applications. In Section 2, we describe a basic method, which is first presented in [30]. With this method, we can compute phase CGHs whose discrete Fourier transforms (DFTs) are exactly controlled on half of the samples, such as even (or odd) indexed rows (or columns). The method requires only a single FFT and trivial arithmetic operations. In Section 3, we supplement the basic method by the application of structured non-random initial phase terms on a desired image. In this way, we reduce encoding noise while keeping speckle noise low and get high quality reconstructions under temporal averaging. Section 4 shows the

experimental results with a commercially available phase-only SLM and Section 5 is reserved for discussions and conclusions.

2. Basic phase CGH computation method

We assume that images are projected at a Fourier plane of the SLM, hence the field distributions on the hologram and the output planes are related by a Fourier Transform (FT). We present the analysis for the 2-f setup shown in Fig. 1(a). Extensions to other FT configurations are straightforward. The SLM (assumed to be pixellated) is placed at the left focal (hologram) plane and is illuminated with a normally incident plane wave. The pixel values of the SLM are denoted by $H_{m,n}$. The resulting analog field on the right focal (output) plane is denoted by $s(x,y)$. Due to the pixellated nature of SLM, $s(x,y)$ is periodic (under the assumptions of impulsive pixels and Fresnel diffraction) with periods $\frac{\lambda f}{\Delta_x} \times \frac{\lambda f}{\Delta_y}$, where f denotes the focal length of the Fourier lens, λ denotes the wavelength and Δ_x, Δ_y denote the SLM pixel periods in x and y directions, respectively. $s(x,y)$ can be uniquely controlled over only one period, which we call the central diffraction order (CDO). The remaining regions of the output plane merely consist of higher order replicas of the CDO with no additional information. If the SLM has $M \times N$ pixels, $s(x,y)$ is also completely specified by its $M \times N$ samples taken within the CDO, with intervals $\frac{\lambda f}{M\Delta_x}, \frac{\lambda f}{N\Delta_y}$. Letting $S_{k,l}$ denote these samples, we have

$$S_{k,l} = \mathbf{DFT}\{H_{m,n}\}. \quad (1)$$

From now on, we drop the index subscripts, hence H denotes the SLM pixel values and S denotes the samples of the output field within the CDO.

For an arbitrary S , H is in general full complex. Thus, if we had a full-complex SLM with a very high dynamic range, we could fully reconstruct any given S . In case of a phase-only SLM though, we in general can not reconstruct S fully. However, a phase-only SLM should be able to (and indeed can) control (reconstruct) $MN/2$ samples of S exactly. This follows from the well-known fact that a complex number \vec{H} with $|\vec{H}| \leq 2$ can be expressed as the summation of two unit magnitude complex numbers [31], i.e., $\vec{H} = \vec{P}_1 + \vec{P}_2$ where $|\vec{P}_1| = |\vec{P}_2| = 1$, as shown in Fig. 1(b). In particular, \vec{P}_1 and \vec{P}_2 can be found as

$$\vec{P}_1 = e^{j(\angle \vec{H} - \alpha)} \quad (2a)$$

$$\vec{P}_2 = e^{j(\angle \vec{H} + \alpha)} \quad (2b)$$

where

$$\alpha = \arccos\left(\frac{|\vec{H}|}{2}\right). \quad (3)$$

Thus, two phase-only pixels of the SLM together constitute one degree of freedom, yielding a total of $MN/2$ degrees of freedom, which should be sufficient for controlling half of S .

We now determine which $MN/2$ samples of S should be targeted. Our concern is that the phase CGH that reconstructs the chosen samples should be determined in a direct manner without any iterations. Figure 2 illustrates our methodology. Figure 2(a) shows a desired S as an $M \times N$ discrete image. Figure 2(b) shows the ideal full-complex $M \times N$ CGH H that generates S . In Fig. 2(b), the upper and lower parts of H are labeled as H_U and H_L , respectively. Both H_U and H_L are $M/2 \times N$ patterns. Next, in Fig. 2(c), S is downsampled such that only the even rows (i.e., rows with even indexes such as $k = 0, 2, 4, \dots$) are preserved and odd rows are zeroed. This downsampling as well-known implies aliasing in the Inverse DFT domain, as illustrated in Fig. 2(d). In particular, upper and lower parts of H are overlapped and superposed. Conversely,

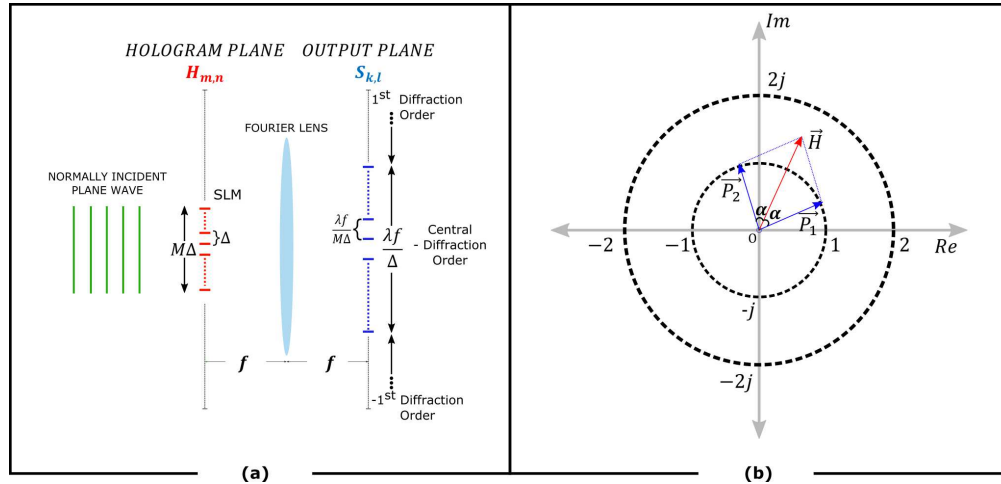


Fig. 1. a) 2-f setup for holographic image projection (HIP) with a spatial light modulator (SLM). b) Decomposition of an arbitrary complex number \vec{H} (with $|\vec{H}| \leq 2$) as the summation of two unit magnitude (phase-only) numbers \vec{P}_1 and \vec{P}_2 , showing that two phase-only pixels constitute one degree of freedom.

the CGH in Fig. 2(d) is the CGH that generates the output samples in Fig. 2(c). Thus, when only the even rows of S are of concern, it is $H_U + H_L$ that matters, and the individual H_U and H_L does not matter. Figure 2(e) and Fig. 2(f) illustrate the dual case of downsampling of odd rows, and show that when odd rows of S are of concern, it is only $H_U - H_L$ that matters. Here, H_L is weighted with a negative coefficient as a result of the one unit downward shift of the impulse train in Fig. 2(e). Finally, Fig. 2(h) shows an $M \times N$ phase CGH which satisfies the condition $P_U + P_L = H_U + H_L$. Here, we assume that $|H_U + H_L| \leq 2$ (which can be achieved with a trivial normalization of H). For each pixel of $H_U + H_L$, we can find \vec{P}_1 and \vec{P}_2 according to Eqs. (2) and (3). Then we can set one of P_U, P_L to \vec{P}_1 and the other to \vec{P}_2 . By Fig. 2(c) and Fig. 2(d), the phase CGH in Fig. 2(h) reconstructs the same even rows with H , as in Fig. 2(g). Hence, if the target samples are chosen as the samples on even rows, they can be exactly controlled via a phase CGH computed without any iterations. Note also that although the phase CGH in Fig. 2(h) reconstructs even rows of S exactly, it in general does not reconstruct the odd rows because $P_U - P_L$ is not necessarily equal to $H_U - H_L$. Indeed, in general, one can select P_U and P_L to satisfy either of the conditions $P_U + P_L = H_U + H_L$ or $P_U - P_L = H_U - H_L$, but not both. Hence, odd rows in Fig. 2(g) are set in an uncontrolled manner, and the reconstruction is degraded by a noise term given by $(H_U - H_L) - (P_U - P_L)$. Figure 2(i) and Fig. 2(j) show the case where the phase CGH perfectly reconstructs odd rows and leaves even rows noisy. In a straightforward manner, the idea can be extended to perfectly reconstruct even or odd columns. In this case, CGHs are split into two halves in the horizontal direction.

In summary, we have developed a method that computes a phase CGH that perfectly reconstructs half of S via a single FFT and trivial arithmetic operations. The simulations in Fig. 3 verify the method, and at the same time illustrate the first attempt for its usage in HIP. Figure 3(a) shows the magnitude of a desired S . The phase, not illustrated, is assigned randomly. Figure 3(b) shows the corresponding ideal CGH, H (magnitude). Figure 3(c) shows a phase CGH designed to reproduce the even rows (phase is shown as a gray scale image with black and white pixels denoting no and full 2π phase modulation, respectively). Figure 3(d) shows the generated S . As seen, even rows are perfectly reconstructed. Odd rows however, are left

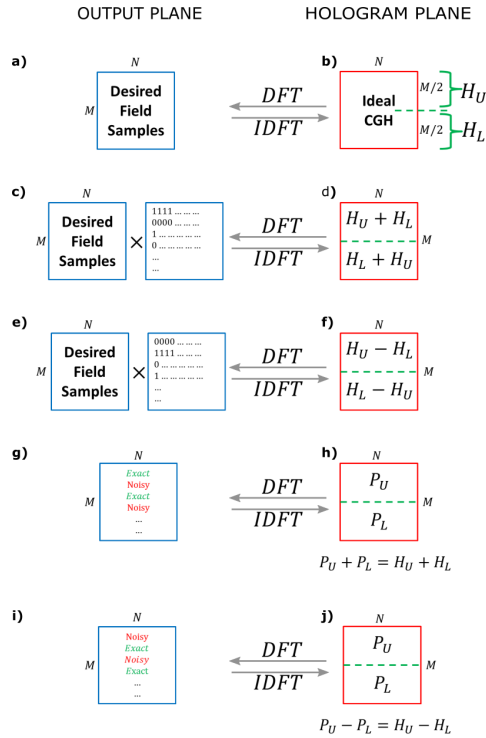


Fig. 2. Basics of the proposed phase CGH computation method. All signals are discrete. a) Desired field S . b) Ideal full-complex CGH H with two halves named H_U and H_L . c) Downsampling of S . Only even rows (rows with even index such as $k = 0, 2, \dots$) are preserved. d) Corresponding CGH, aliased as a result of downsampling. e) Downsampling of S . Only odd rows are preserved. f) Corresponding CGH. h) A phase CGH satisfying $P_U + P_L = H_U + H_L$ ($|H_U + H_L| \leq 2$), computed as in Fig. 1(b). g) The field generated by h. In accordance with c and d, h generates the same even rows with H . Odd rows however are left uncontrolled and appear noisy. i-j) Counterpart of g-h for perfect reconstruction of odd rows. Phase CGHs exactly control half of the degrees of freedom, as expected.

uncontrolled and appear noisy. Figure 3(e) and Fig. 3(f) show the dual case where odd rows are perfectly reconstructed and even rows appear noisy.

One disadvantage of the presented method, as evident in Fig. 3, is that the signal and noise samples are interlaced into each other. Thus, in the output, the encoding noise appears distributed and the reconstructed images appear highly noisy. It would have been better if the controlled half of the samples were grouped together within a signal window, and the uncontrolled half were grouped together within a noise window. However, to our knowledge, a direct non-iterative solution for that case is not possible. Fortunately, it is possible to further tailor the basic method such that the effect of the encoding noise is reduced. We explore that possibility in the next section.

An important requirement of the proposed method is that the illumination wave should have a uniform intensity over the SLM. The reason is, the entire method relies upon the assumption that unit magnitude pixels in the two halves (upper and lower, or left and right) of the phase-only SLM are superposed to form complex-valued pixels. If the actual illumination is not uniform, different complex pixel values are realized, and we get additional noise on the reconstructions. Of course, the entire illumination wave should have the necessary degree of spatial and temporal

coherence so that the light from two halves of the SLM interfere.

We finally note that for sake of clarity, we explained our method for a 2-f setup. If it is desired to free the system of any lenses, one option is to perform reconstructions at the far field, where the Fraunhofer diffraction formula applies. For closer distances where the wave distributions on SLM and image planes are related by Fresnel diffraction formulas, the proposed method still works if phase CGHs are multiplied by QPF terms that undo the pre-multiplicative chirp term of Fresnel diffraction [32].

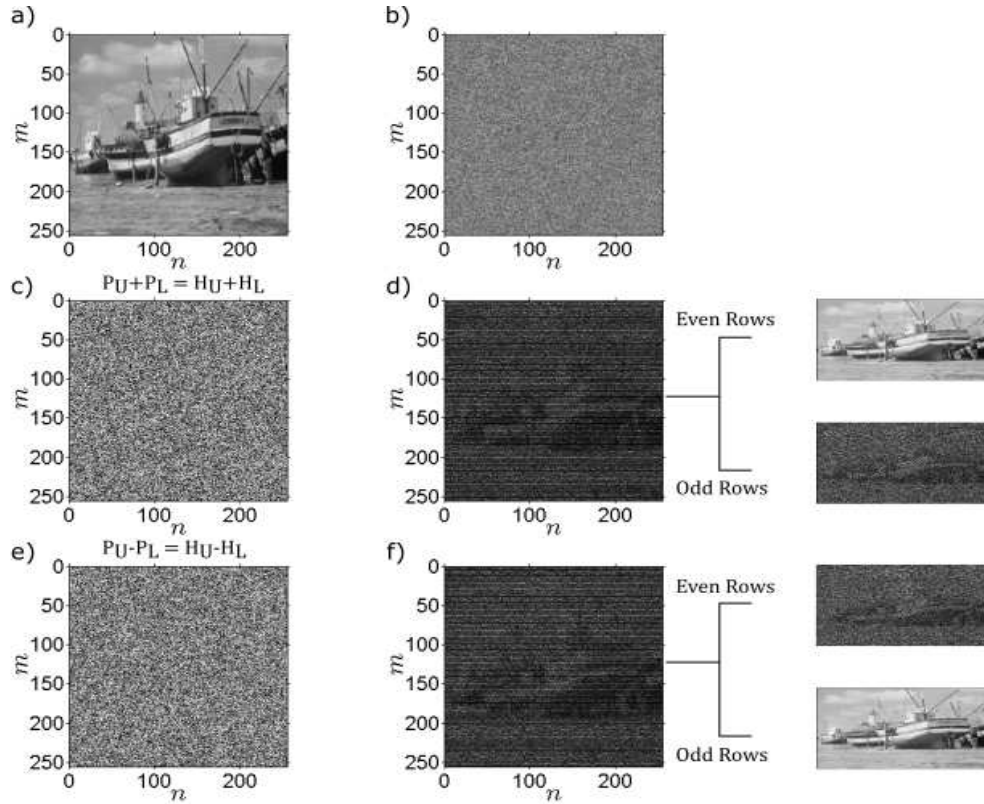


Fig. 3. Verification of the basic phase CGH computation method. (a) Desired field S . Only magnitude is shown. Phase is random. (b) Magnitude of ideal full-complex CGH H . (c) Phase CGH satisfying $P_U + P_L = H_U + H_L$, shown as a gray scale image. (d) Reconstruction of c and its downsampled versions. (e) Counterpart of c-d for phase CGH satisfying $P_U - P_L = H_U - H_L$.

3. Application to holographic image projection

In HIP, we wish to set the intensity distribution on the Fourier plane of the phase-only SLM to that of a desired image. We examine two different cases that are illustrated in Fig. 4. In the first case, we target the entire CDO region (with area $\frac{\lambda f}{\Delta_x} \times \frac{\lambda f}{\Delta_y}$), i.e., the desired image extends over a full period. In the second case, we target only half-of the CDO (with area $\frac{\lambda f}{2\Delta_x} \times \frac{\lambda f}{\Delta_y}$ or vice versa) and confine the desired image here. The other half is used as a don't care region and reserved for the encoding noise. The first case is advantageous in terms of light efficiency, while the second case enables the achievement of lower reconstruction error. In both cases, we eventually use

the basic method described in Section 2. However, we apply initial phase distributions on the desired image prior to the application of the basic method in order to keep the encoding noise low. The initial phase distributions also provide speckle reduction. We also discuss strategies in which we calculate multiple phase CGHs for a given image, display them time sequentially, and make use of temporal averaging to further improve quality of the reconstruction.

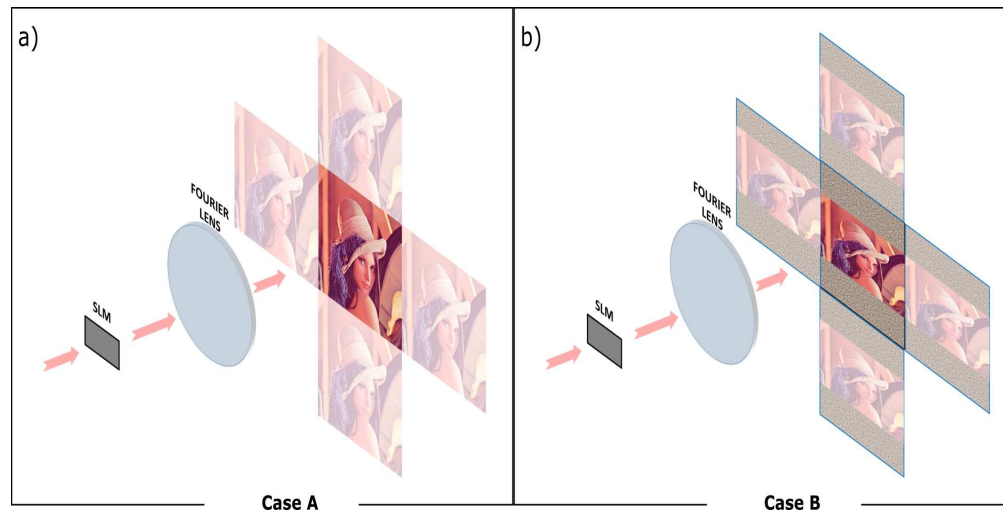


Fig. 4. Examined HIP scenarios. (a) Desired image is specified over the entire central diffraction order (CDO). Phase freedom on the image plane is exploited to decrease encoding error. (b) Desired image is specified over half of the CDO. The unused part of CDO is reserved for encoding noise.

3.1. Case A: Image extends over the entire CDO

When the entire CDO is used as the image area, the only way to mitigate the CGH encoding noise is to make use of the phase-freedom on the image plane [10, 29, 33]. Phase terms applied on the target images are designed to create a more uniform energy distribution on the SLM plane. In that way, encoding noise is reduced. Similar to the case in Fig. 3, most algorithms apply a random phase distribution which leads to high speckle noise. Recently, Shimobaba et al. proposed the application of a quadratic phase function (QPF) rather than a random phase term [34, 35]. Their QPF term essentially maps the diffracted version of the target image in a 1-1 fashion on the SLM. As a result, energy extends over the entire SLM. Subsequently, they apply the Error Diffusion algorithm and get reconstructions with low encoding noise. The non-random nature of their QPF term also leads to reduced speckle noise. Our solution is similar, but with some difference in the applied QPF term. More importantly, in the second stage, rather than Error Diffusion, we apply the basic method presented in Section 2, which is much faster.

We first divide the target image into two parts that have almost the same energy as in Fig. 5(a). We map one of these parts to the upper half of the SLM via a suitably adjusted QPF term. The second part is mapped to the lower part of the SLM via another QPF term. In this way, we ensure that image energy is distributed pretty smoothly over the SLM area, which helps to keep the encoding noise low. The energy based splitting of the desired image, rather than a simpler splitting into two equally sized sub-images, is preferred here to handle cases where one-half of the image has significantly lower energy compared to the other. We also adjust the QPF terms such that some safety region is left at the boundary between the two halves of the SLM. In

particular, the middle rows of the SLM do not carry significant information. In this way, we ensure that the harsh aperture windows that we apply when extracting H_U and H_L out of H do not cause significant diffraction artifacts. Finally, we apply the basic method in Section 2 on H and determine a phase CGH. Here, we do not shuffle \bar{P}_1 and \bar{P}_2 among P_U and P_L , but we orderly set all pixels of P_U to \bar{P}_1 and all pixels of P_L to \bar{P}_2 (or vice versa) as shown in Fig. 6(a). In this way, we ensure that the encoding noise on the odd rows has a low-pass nature and is better controlled. Figure 7(a) shows a desired image, and Fig. 7(b) shows the corresponding ideal full-complex CGH obtained as described above. Figure 7(d) shows the reconstruction performed by a phase CGH designed to perfectly reconstruct the even rows. Thanks to the applied initial phase term, the encoding noise distributed on the odd rows has reduced effect on the overall image. Speckle noise is also reduced.

The idea can be extended to phase CGHs for even or odd columns in a straightforward manner. In that case, the desired image and the SLM is split into two parts horizontally, rather than vertically, and QPF terms are modified accordingly. Figure 7(c) shows the ideal full-complex CGH for the column case, and Fig. 7(e) shows the reconstruction when phase CGH is computed for even columns.

Careful examination of Fig. 7(d) and Fig. 7(e) reveal that although the effects of encoding and speckle noise are reduced, some ghost replica artifacts are present in the reconstructions. Such artifacts occur as a consequence of the mixing performed between the two halves of the SLM when computing the phase CGHs, and appear dominantly on the reconstruction when only a single phase CGH is used per a desired image. However, further improvements can be achieved by exploiting the finite temporal response time of the human visual system. In particular, for a given desired image, more than one CGH can be computed such that each CGH reconstructs one of even rows, odd rows, even columns and odd columns perfectly. Then these CGHs can be displayed time sequentially and temporally averaged. Figure 7(f)-7(h) show temporally averaged reconstructions for different combinations of two or four CGHs. As seen, the encoding noise is smoothed further, but at the cost of divided SLM frame rate.

The reader can truly claim that any CGH computation method (including the simplest direct quantization method) can have an improved error performance when temporal averaging is allowed, and may wonder what difference our method has in comparison. Actually, our method makes more efficient use of temporal averaging compared to other methods. To see this, consider a CGH computed for even rows. The image generated by this CGH has a high error partly due to the fact that the information on the odd rows is discarded [Fig. 7(d)]. That missing piece of information is restored if a second CGH is computed for odd rows, and used in conjunction with the first CGH in a time averaged fashion [Fig. 7(f)]. In other words, time averaging not only smooths out encoding noise, but also completes the information content. Therefore, the improvement in error is stronger. Temporal averaging of two row CGHs provide significant improvement over a single CGH, but actually a set of four CGHs that include the column CGHs as well is better. The reason is, the ghost replica artifacts for even and odd row CGHs appear at the same locations, and hence appear persistent even under temporal averaging. However, the ghosts of column CGHs appear at different positions [Fig. 7(g)]. So, if they are included in the time-averaging process, the effect of the artifact is reduced [Fig. 7(h)]. We also note that although we compute four CGHs, the computation requires only two FFT operations, one for row CGHs, one for column CGHs. Hence, computational efficiency of the algorithm is still preserved.

Table 1 reports the performance of the proposed algorithm under different temporal averaging schemes. For each case, the algorithm is applied on a test set including the well-known *Lena*, *Cameraman*, *Boat*, *Peppers*, *Mandrill* images, and the average mean-squared error (MSE) [20] and structured similarity index measure (SSIM) [36] values are reported, along with the re-

quired number of FFT operations per image (not per reconstruction) and the demanded SLM frame rate to deliver a monochrome video with a frame rate specified by \mathbf{F} . Image quality improves as more reconstructions are averaged, with the 4-average case performing the best. Table 2 provides a comparison of our 4-average algorithm with the Iterative Fourier Transform Algorithm (IFTA), which is generally known to yield the best error performance. Each row of Table 2 specifies the number of reconstructions to be averaged per image and the number of IFTA iterations required for each reconstruction, such that the MSE performance of the 4-average case is achieved. The indicated iteration numbers are again averaged over the above-mentioned image set. Also note here that the third column of Table 2 is reported by taking into account that IFTA requires two FFTs per iteration. Tables 1 and 2 clearly highlight the high computational efficiency of our solution.

In closure, we note that the level of the ghost replica and ringing artifacts can be further reduced by performing a small number of IFTA iterations on the phase CGHs obtained with our method. In terms of computational complexity, this strategy slightly hinders the advantage of our non-iterative method, but is still better compared to IFTA solutions starting from random initial CGHs since our phase CGHs already have a low error, enabling faster convergence. Increasing the number of IFTA iterations used per phase CGH, the required number of temporal averages hence the SLM frame rate can be decreased as well. Thus, a trade-off between required SLM frame rate, reconstruction quality and computational complexity can be established. We also remind that the artifacts are a result of our speckle reduction goal (i.e. the artifacts only appear in Fig. 7 where we use structured initial phase terms, but do not appear in Fig. 3 where we use random phase terms). If some controlled amount of randomness is allowed on the initial phase terms applied on the images, the level of artifacts can be reduced at the expense of increased speckle noise as well.

Table 1. Performance of the proposed HIP algorithm for Case A. The average Mean Squared Error (MSE) and Structured Similarity Index Measure (SSIM) values of a set of desired images is reported.

Number of Reconstructions per Image	MSE (%) (average)	SSIM ($max: 1$) (average)	Number of FFT per Image	Required SLM fps (\mathbf{F} : video fps)
1	47.3	0.31	1	\mathbf{F}
2	21.9	0.44	1	$\mathbf{F} \times 2$
4	12.3	0.52	2	$\mathbf{F} \times 4$

Table 2. IFTA configurations that achieve the MSE performance of the last row of Table 1.

Number of Reconstructions per Image	Number of Iterations per Reconstruction (average)	Number of FFT per Image (average)	Required SLM fps (\mathbf{F} : video fps)
1	> 60	> 60	\mathbf{F}
2	10.8	43.2	$\mathbf{F} \times 2$
3	3.4	20.4	$\mathbf{F} \times 3$
4	1.5	12	$\mathbf{F} \times 4$

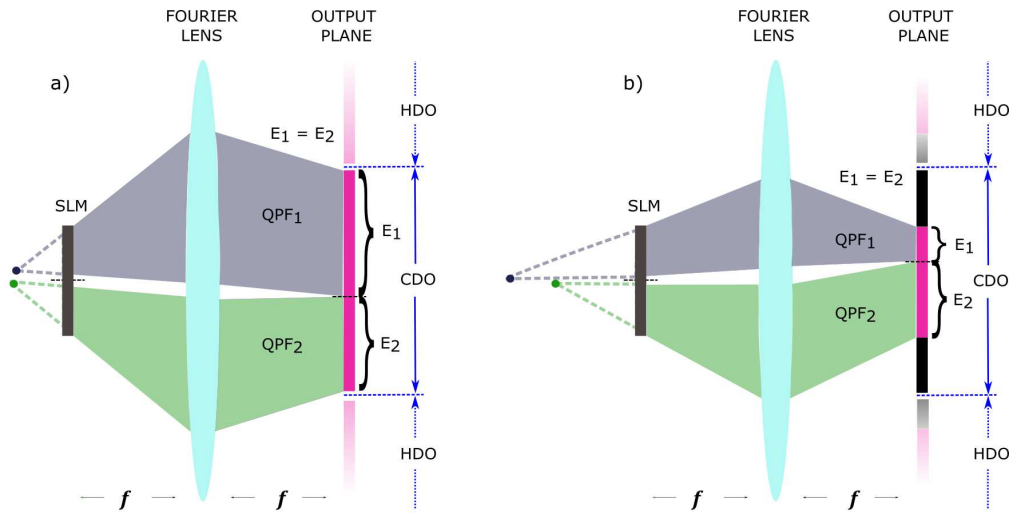


Fig. 5. Initial phase terms (Quadratic Phase Functions - QPF) applied on the desired images to obtain a smooth energy distribution on the SLM plane. Desired image occupies (a) the entire CDO, (b) half of the CDO. In both cases, desired image is split into two parts with almost equal energies E_1 and E_2 . In general, the two parts have different sizes. The upper (lower) part is mapped to upper (lower) half of the SLM via a suitable QPF term, which actually acts as a lens term that locally adjusts the ray directions for the mapping. In this way, image energy is distributed uniformly on the SLM, enabling a low encoding noise. The middle region of the SLM is left relatively empty to avoid diffraction artifacts during the calculation of phase CGHs.

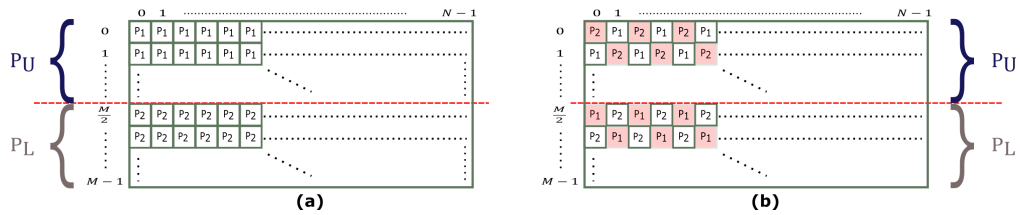


Fig. 6. Assignment of \vec{P}_1 and \vec{P}_2 to P_U and P_L in (a) Case A (b) Case B, where pixels on a checkerboard pattern are flipped with respect to Case A.

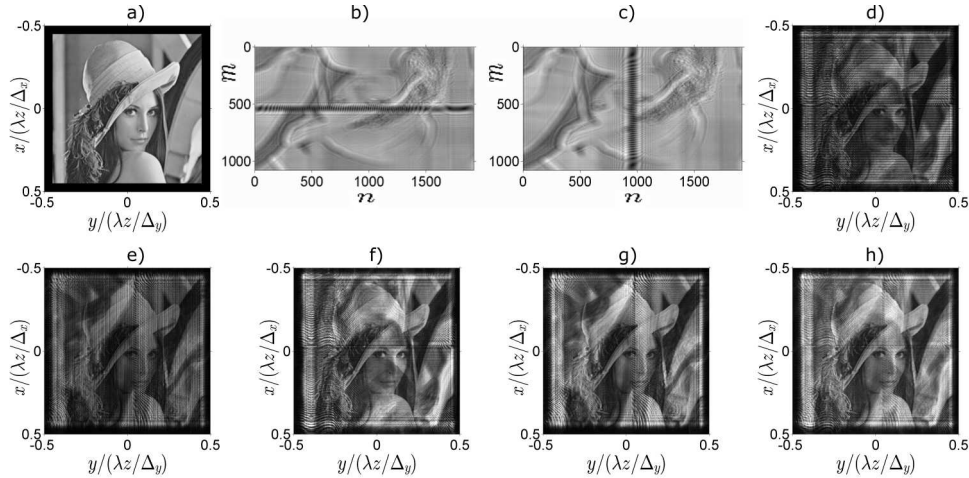


Fig. 7. Simulation results for *Case A*. a) Desired image specified within the entire CDO. b,c) Ideal full-complex CGHs respectively for the row and column cases, obtained by the application of the QPF terms in Fig.5(a). d,e) Reconstructions by phase CGHs designed respectively for even rows and even columns. Reconstructions by phase CGHs for odd rows and columns look similar. f) Time averaged reconstruction by two phase CGHs designed for even and odd rows. g) Time averaged reconstruction by two phase CGHs designed for even and odd columns. In f and g, two SLM frames are required to form each video frame. h) The average of f and g, requiring 4 SLM frames per video frame. In d and e, there are missing pixels and artifacts, hence reconstruction error is high. Note also that the artifacts in d and e appear at different locations. In f and g, information is completed, but artifacts appear persistent since only reconstructions by row or column type CGHs are averaged. In h, information is complete and artifacts are relatively suppressed, hence best image quality is achieved.

3.2. Case B: Image occupies half of the CDO

When only half of the CDO is used for image projection, the unused half can be used to distribute the encoding noise. Therefore, compared to Case A, images with much lower error values can be expected. Phase CGHs for this case are mostly computed with the Fineup with Don't Care (FIDOC) or Direct Search algorithms, which are again iterative [10, 20, 22, 24, 26]. We now show that our non-iterative basic method can also be extended to this case. Figure 8(a) shows a desired image that occupies merely half of the CDO. We apply two QPF terms to this image and distribute it on the SLM area as in the previous case [Fig. 5(b)]. The QPF terms are designed for the column case, and are adjusted to handle the smaller image area. Figure 8(b) shows the resulting H . Next, we compute the phase CGH for even columns. At this stage however, we make the following change relative to Case A: if $m + n$ is even, we flip \vec{P}_1 and \vec{P}_2 , as shown in Fig. 6(b). If $m + n$ is odd, we make no changes. This modification is inconsequential when sum of pixels is considered. Therefore, even columns are still reproduced exactly. However, difference of pixels is changed, thus the odd columns generated by the CGH are changed. The high-frequency modulation we impose shifts the encoding noise from the image area to the unused portions of the CDO, as evident in the reconstruction provided in Fig. 8(c). The image area receives quite minor contribution from encoding noise. The reconstructed image appears fine, but has high error due to the fact that odd rows are missing ($MSE = 33\%$, $SSIM = 0.69$). To complete the image, we compute a second CGH for odd columns. When the two CGHs are displayed time sequentially, we obtain the time-averaged image shown in Fig. 8(e). The image

has a high quality and a quite low error ($MSE = 3\%$, $SSIM = 0.76$). On the contrary to the previous case, four CGHs are not needed in time averaging, but two CGHs suffice, since ghost replica artifacts appear in the unused areas of CDO.

To provide a comparison, we applied our time-averaged solution (two SLM frames and 1 FFT for each image) and the FIDOC algorithm (1 SLM frame per image, 2 FFT per iteration) on the image set used in Case A. The average MSE error with our solution is 2.9%, while the same MSE performance requires on the average 10.6 iterations (corresponding to 21.2 FFTs per image) with the FIDOC algorithm. When two FIDOC reconstructions are temporally averaged, we require on the average 5.2 iterations to be performed per reconstruction to match the MSE value of our proposed method (yielding a similar demand of $2 \times 2 \times 5.2 = 20.8$ FFTs per image).

4. Experimental results

We carried out proof of concept HIP experiments with the setup illustrated in Fig. 9(a) to verify our CGH computation algorithm. The light source is a He-Ne laser and the computed phase CGHs are displayed on a Holoeye-Pluto SLM having $8 \mu m$ pixel pitch and 8-bit modulation depth. The modulated light beam coming out of the SLM is directly projected onto the CCD array of a camera without any spatial filtering. The camera is placed slightly off-axis to avoid the unmodulated (i.e. direct, DC) beam of the SLM. A linear phase term is superimposed on the phase CGHs to perform off-axis reconstructions.

Figure 9(b) shows the experimental result for Case A of Section 3 where the desired image occupies the entire CDO. The image is obtained as the average of the reconstructions of four phase CGHs computed for even/odd rows/columns. Figure 9(c) shows the result for Case B of Section 3 where the desired image is limited to half of the CDO. This time, we show the average of the reconstructions of only two CGHs. Although the experimental results verify the presented algorithm, there is some discrepancy and loss in image quality in comparison to the simulation results in Fig. 7 and Fig. 8, which is attributed to the non-idealities of the SLM, such as pixel cross-talk and flickering of liquid crystal cells.

To provide a comparison of image quality, Fig. 9(d) shows the counterpart of Fig. 9(b) obtained with IFTA algorithm (average of 4 reconstructions, 2 iterations per reconstruction). It is clearly seen that our method significantly reduces the speckle noise, however, at the cost of some ghost replica or ringing artifacts. A counterpart of Fig. 9(c) with FIDOC algorithm is not provided, since the image appearance is almost the same, although with our algorithm computation is much faster.

5. Conclusion

In this paper, we present a fast non-iterative algorithm to compute phase CGHs for HIP. The greatest advantage of the solution is its quite low computational complexity that well complies with real-time applications. In the examined cases in Section 3, Case A requires only a single FFT operation per color channel of a video frame if at most two reconstructions are temporally averaged. If four reconstructions are averaged, two FFTs are needed. In Case B, high image quality readily requires at most two reconstructions to be averaged, so only a single FFT needs to be performed per color channel of a video frame. Another merit of our algorithm is the low speckle noise achieved by the non-random, structured initial phase terms applied on the images.

When current-state of the art phase-only SLM technology and the available frame rates of 60 Hz are considered, it seems that Case B of Section 3 has the highest practical applicability potential. 60 fps interlaced video format (in which only half of the spatial resolution is available for each video frame) can be readily delivered with our solution for case B without any frame rate division (of course, color video requires 3 SLMs). The other cases we explored require SLMs with higher frame rates and are more likely to be useful in the future. High quality 60 fps

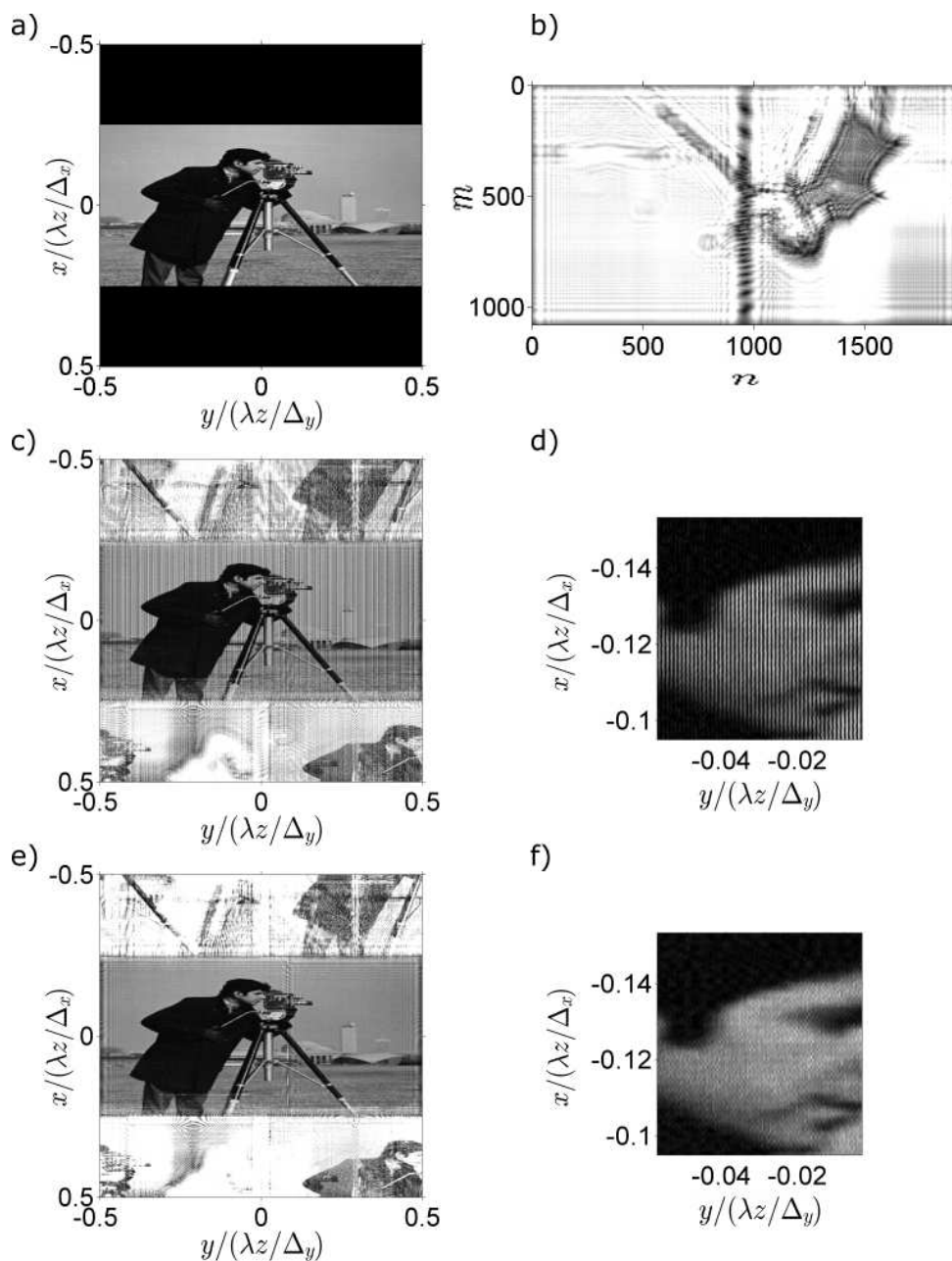


Fig. 8. Simulation results of *Case B*. (a) Desired image within the CDO. Dark regions are reserved for encoding noise. (b) Corresponding ideal full-complex CGH, obtained by the application of the QPF terms in Fig.5(b). (c) Reconstruction by a phase CGH designed for even columns. Encoding noise mainly appears in the unused part of CDO, and odd columns within the image area appear as missing, rather than noisy, similar to that in interlaced video format. (d) Zoom-in version of c. (e) Average of the reconstructions of two phase CGHs for even and odd columns. (f) Zoom-in version of (e). In e and f, full information is restored, and speckle and encoding noise is quite low.

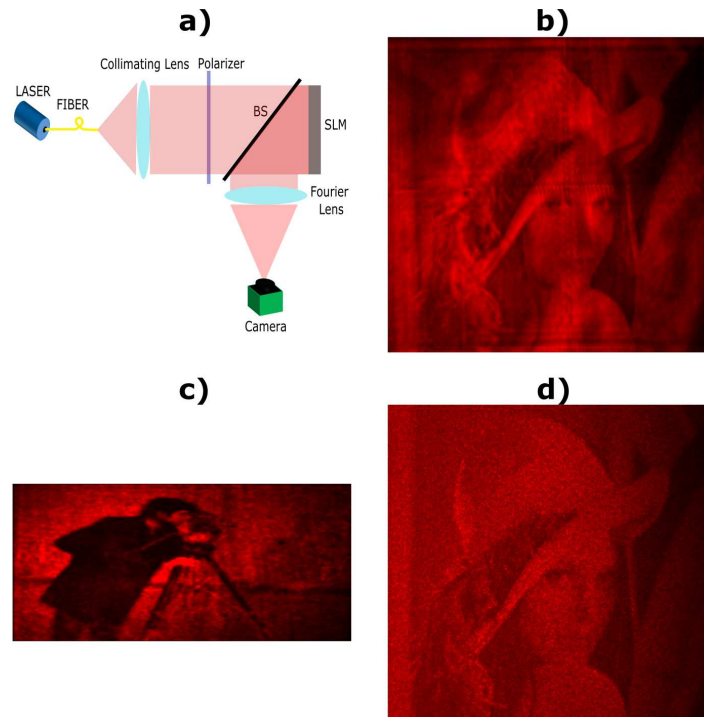


Fig. 9. a) Experimental HIP setup. Camera is placed slightly off-axis to avoid the unmodulated beam of the SLM. b) HIP Case A, average of reconstructions of four phase CGHs. Experimental version of Fig. 7(f). c) HIP Case B, average of reconstructions of two phase CGHs. Experimental version of Fig. 8(e). The lower quality in comparison to simulation results is due to SLM pixel cross-talk and flicker effects. d) HIP Case A obtained with IFTA algorithm, which makes the speckle reduction ability of our algorithm quite evident.

progressive video requires 2 and 4 reconstructions per color channel to be averaged respectively for case B and A, implying SLM frame rates of 120 and 240 Hz per color. Such high frame rates are not possible with the current LCoS phase-SLM technology, but may be attained with newly emerging blue-phase materials [37]. Standard cinema quality low-persistence video operating at 24 fps though requires SLM frame rates of 48 or 96 Hz for each color, which is more likely to be attained.

Despite its high frame rate requirements, Case A is advantageous in that it operates with maximum light efficiency. For this case, under the assumption that the light source already generates polarized light, our simulations indicate a light efficiency of approximately 60%, where light is lost only to the unmodulated beam of the SLM and higher diffraction orders. In case B though, a significant part of the energy appears as encoding noise, decreasing the light efficiency to about 6%. However, we remind that such low efficiency values are also the case in alternative algorithms, so our algorithm does not impose a disadvantage here.

Acknowledgments

This research has been supported by European Research Council, ERC Advanced Grant Wear3D, 340200.